Autoresonant Dynamics of Optical Guided Waves

Assaf Barak,[1] Yuval Lamhot,[1] Lazar Friedland,[2] and Mordechai Segev[1]
[1]*Physics Department, Technion - Israel Institute of Technology, Haifa 32000, Israel*
[2]*Racah Institute of Physics, Hebrew University of Jerusalem, Jerusalem 91904, Israel*
(Received 15 March 2009; published 14 September 2009)

We study, theoretically and experimentally, autoresonant dynamics of optical waves in a spatially chirped nonlinear directional coupler. We show that adiabatic passage through a linear resonance in a weakly coupled light-wave system yields a sharp threshold transition to nonlinear phase locking and amplification to predetermined amplitudes. This constitutes the first observation of autoresonance phenomena in optics.

DOI: 10.1103/PhysRevLett.103.123901 PACS numbers: 42.65.Sf, 42.65.Wi, 52.35.Mw

Autoresonance is a fascinating nonlinear phenomenon in which a system is captured into continuous resonance, remaining phase locked with driving oscillations (or waves) despite variations in the system parameters. For intuition, imagine a system where one wave amplifies another. Naturally, for efficient amplification the waves should propagate in a phase-matched fashion; otherwise power can flow back to the pump. Modern nonlinear optics goes a long way to ensure phase matching, employing birefringence, periodic poling, etc. But what would happen if the system parameters vary during propagation? One could engineer phase-matched conditions in a predesigned way, but this would work only if the system parameters vary in a known fashion. Is there a way that a dynamic system, where one wave amplifies another, could self-lock in resonance even if the system parameters vary considerably? The phenomenon called autoresonance does just that: it uses the nonlinearity of the system to lock in resonance, and maintain efficient amplification despite considerable variations of system parameters. Here, we introduce and experimentally demonstrate, autoresonance in nonlinear optics.

Let us first briefly describe autoresonance. Generally, when trying to excite a resonant system with large variations of parameters deeply into the nonlinear regime, one has to use some feedback control or tailor the external driving oscillations precisely to remain in resonance continuously. Otherwise the system detunes from resonance since its resonant frequency varies considerably. Autoresonance offers a different way to maintain phase locking even when the system is excited deeply into the nonlinear regime. When a nonlinear oscillator is driven adiabatically through its linear resonance, it phase locks with the driver and, above a sharp threshold, maintains the phase locking despite considerable variations in the system parameters. Such phase locking is a fully nonlinear process, and occurs because the nonlinear oscillator slowly self-adjusts (in amplitude, frequency, etc.) to maintain the resonance. Autoresonant dynamics was studied in many systems such as plasma [1], particle accelerators [2], fluid dynamics [3], solitons [4], controlled excitation of atoms [5], BEC condensates [6], superconducting Josephson junctions [7] and more. In addition, autoresonance was studied theoretically in a general three wave mixing paradigm [8]. However, autoresonance was never observed experimentally in optics, nor was autoresonant amplification of optical waves ever studied theoretically in any optical context. This is in spite of the fact that phase locking is highly important in many optical processes. For example, phase locking plays a major role in nonlinear frequency conversion, high harmonics generation, waveguide arrays, Raman scattering, coupled oscillators and more.

Here, we present the first observation of autoresonance in optics. We study the dynamics of coupled waves passing adiabatically through a linear resonance of a nonlinear directional coupler (double-well potential). We show that in this system of driving and driven waves, above a sharp threshold, the driven wave adjusts itself continuously, assisted by the nonlinearity, to stay phase locked with the driving wave despite variations in the potential.

Consider a coupler in which one of the waveguides is chirped (its refractive index increases monotonically in the propagation direction), and the medium exhibits Kerr nonlinearity. A pump wave is launched into the chirped waveguide, with zero input into the second waveguide. The evolution of a monochromatic beam of envelope ψ in (1 + 1)D is described by the dimensionless nonlinear Schrödinger equation (NLSE):

$$-i\partial\psi/\partial z = \partial^2\psi/\partial x^2 + [\Delta n_L(x,z) + |\psi|^2]\psi. \quad (1)$$

Our system includes two coupled waveguides: the left one is propagation invariant, while the right one is spatially chirped. The linear resonance is obtained when the refractive index profiles (linear + nonlinear) of the two waveguides are identical. In resonance, the coupling between the waveguides is most efficient, whereas when they are detuned, the coupling efficiency decreases [9]. The linear refractive index profile [Fig. 1(a)] is described by $\Delta n_L(x,z) = \Delta n_1(x) + \Delta n_2(x)q(z)$, where $\Delta n_1(x)$ represents a z-invariant symmetric coupler profile, $\Delta n_2(x)$ describes the shape of the right waveguide only. For concreteness, we take $q(z) = \alpha z$ to be a sufficiently slow

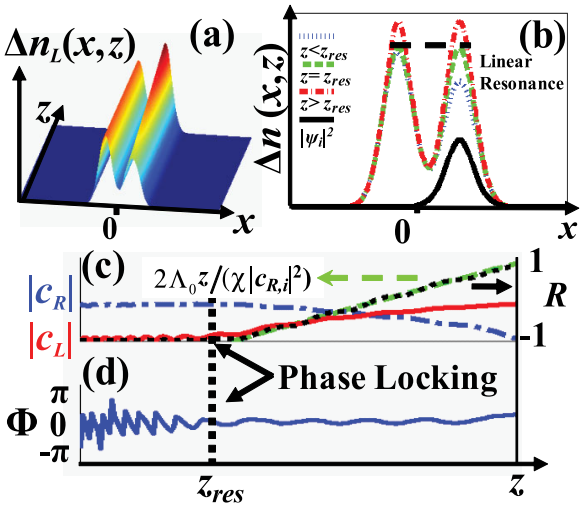

FIG. 1 (color online). (a) The linear refractive index profile defining the chirped directional-coupler, $\Delta n_L(x, z)$. (b) Total refractive index profile (linear + nonlinear) at various propagation planes, before resonance crossing (blue dotted line), at the crossing (green dashed line), and beyond the crossing (red dotted-dashed line). Black solid line depicts the initial wave packet, ψ_i. Horizontal black dashed line marks the linear resonance. (c) Evolution of $|c_R|$ (blue dotted-dashed line), $|c_L|$ (red solid line), R (black dotted line), and the theoretically predicted dependence $R = 2\Lambda_0 z/(\chi|c_{R,i}|^2)$ (green dashed line). (d) Evolution of the phase mismatch, Φ. As the system crosses the linear resonance marked with vertical dotted black line, Φ locks near zero and R changes from -1 to nearly 1.

function of z, where α is the linear spatial chirp rate, and $-1/\alpha < z$ for all lengths z in the structure. Under proper conditions, one can use coupled-mode (perturbation) theory to get solutions of the form: $\psi = \exp(i\beta_0 z) \times [c_R(z)u_R(x) + c_L(z)u_L(x)]$, where u_R (u_L) is the eigenmode of the single right (left) waveguide in the absence of nonlinearity and without the chirp, normalized as: $\int_{-\infty}^{\infty} |u_{R,L}|^2 dx = 1$. We denote $c_{R,L}$ as the complex amplitude of $u_{R,L}$, while $\beta_0 = \int_{-\infty}^{\infty} u_{R,L}^* H_0 u_{R,L} dx$ is the highest propagation constant of a single unperturbed linear waveguide, where $H_0 = \partial^2/\partial x^2 + \Delta n_1(x)$ is the unperturbed Hamiltonian. Substituting ψ into Eq. (1), yields two coupled equations describing the dynamics of c_R and c_L:

$$-i\frac{dc_R}{dz} = \kappa c_L + \frac{\chi}{2}|c_R|^2 c_R + \Lambda_0 c_R z \tag{2a}$$

$$-i\frac{dc_L}{dz} = \kappa c_R + \frac{\chi}{2}|c_L|^2 c_L. \tag{2b}$$

$\kappa = \int_{-\infty}^{\infty} u_R^* H_0 u_L dx$ is the coupling coefficient, $\chi = 2\int_{-\infty}^{\infty} |u_L|^4 dx$ is the effective nonlinearity, and $\Lambda_0 = \alpha \int_{-\infty}^{\infty} |u_R|^2 \Delta n_2(x) dx$ is the effective chirp rate. We launch the initial wave packet, ψ_i, having the spatial shape of u_R [black-solid line in Fig. 1(b)], into the right waveguide. Equation (2) yields, for the fractional population difference $R = \frac{|c_L|^2 - |c_R|^2}{|c_L|^2 + |c_R|^2}$ and the phase mismatch, $\Phi = \theta_R - \theta_L$, where $\theta_{R,L}$ is the phase of $c_{R,L}$

$$\frac{dR}{dz} = -2\kappa\sqrt{1 - R^2}\sin(\Phi), \tag{3a}$$

$$\frac{d\Phi}{dz} = \Lambda_0 z - \frac{1}{2}\chi R|c_{R,i}|^2 + 2\kappa\frac{R}{\sqrt{1 - R^2}}\cos(\Phi). \tag{3b}$$

Here, $|c_{R,i}| = \sqrt{|c_R(z)|^2 + |c_L(z)|^2}$, the amplitude of the wave launched into the right waveguide, is a constant of motion. As long as the refractive index does not cross the linear resonance, most of the power is located in the right waveguide ($|c_R| \gg |c_L|$), which yields $R \approx -1$. The linear resonance crossing occurs when the first two terms on the right-hand side (RHS) of Eq. (3b) cancel each other (i.e., the two waveguides are almost identical). This yields resonance crossing at: $z_{\text{res}} = -\chi|c_{R,i}|^2/(2\Lambda_0)$. Figure 1(b) shows the index profile before the resonance crossing [blue dotted line], at the linear resonance [green dashed line], and beyond resonance [red dotted-dashed line]. After passage through the linear resonance, power tunnels continuously and unidirectionally from the right waveguide to the left one, to keep their refractive indices nearly equal despite the chirp. This is how the system self-adjusts, via the nonlinearity, to maintain resonance. This makes the waveguides almost identical for large propagation distances, until the power in the driving wave is exhausted. The process requires sufficient adiabaticity of the structure. The limiting values on α depend on $|c_{R,i}|$ and on z. The most stringent nontrivial condition on adiabaticity is found in the initial resonant capture stage, where there exists a sharp threshold on $|c_{R,i}|$ for capture into resonance (see [10] for description of this effect in dynamical problems). We find a similar threshold in our system.

Until now, the results are based on the coupled-mode theory. It is instructive, however, to test the theory by a direct simulation. We therefore simulate Eq. (1), using a standard beam propagation code, with the initial condition on ψ equal to the waveform ψ_i [black solid line in Fig. 1(b).]. To facilitate quantitative comparison with the analytics, we project the simulated $\psi(x, z)$ onto $u_{R,L}$ to find $c_{R,L}$. The result is presented in Fig. 1(c), showing the evolution of $|c_R|$ [blue dotted-dashed line], $|c_L|$ [red solid line], and R [black dotted line]. As the system crosses the linear resonance [marked by vertical dotted-black line], the phase mismatch Φ locks near zero (exhibiting only small autoresonant oscillations) [Fig. 1(d)]. This phase locking causes $|c_R|$ to decrease to almost zero, while $|c_L|$ increases to nearly $|c_{R,i}|$, leading to the variation of R from -1 to nearly 1, that is, almost full power exchange [better conversion could be achieved if the chirp rate would decrease with z]. The condition for autoresonant evolution is that the first and second terms on the RHS of Eq. (3b) remain nearly equal throughout propagation [equivalent to the waveguides remaining nearly identical, despite the chirp]. This condition predetermines the evolution of $R : R \approx 2\Lambda_0 z/(\chi|c_{R,i}|^2)$ [green dashed line in Fig. 1(c)]. We emphasize that this is the averaged evolution, while the actual dependence of R on z also involves small superimposed os-

cillations with amplitude and frequency scaling as $\kappa^{1/2}$ [10].

As noted above, autoresonance has a sharp threshold depending on the characteristic rates in the system [10]. It is convenient to define a dimensionless threshold parameter $T = 2.45\kappa(\chi)^{1/2}|c_{R,i}|(\Lambda_0)^{-3/4}$, where $\kappa(\chi)^{1/2}|c_{R,i}|$ is related to the rate of nonlinear index changes in the left waveguide, and Λ_0 describes the chirp rate in the right waveguide. The transition to autoresonance occurs at $T = 1$. This threshold can be realized by controlling $|c_{R,i}|$. Figures 2(a) and 2(b) show the evolution of $|\psi|^2$ below and above threshold, respectively [white dashed line marks the linear resonance crossing]. Clearly, below threshold almost no power tunnels to the left waveguide, whereas above threshold all the power is transmitted. This tunneling process is unidirectional, as opposed to a linear directional coupler, where the waveguides exchange power periodically. The unidirectional action here can be understood as follows. At $T < 1$, as the system crosses the linear resonance [Fig. 2(c), vertical black-dashed line], the nonlinear index variation rate in the left waveguide is too slow to follow the changes in the right one; hence, the phases do not lock and power transfer is inefficient [red dashed line in Fig. 2(c)]. However, when $T > 1$ the variation rate of the nonlinear index in the left waveguide is sufficient to follow the changes in the right one, the phases lock and the power tunnels completely from one waveguide to the other [blue solid line in Fig. 2(c)]. As predicted by the theory, the threshold amplitude for autoresonant phase locking, $|c_{R,i}{}^{TH}|$, scales as $(\Lambda_0)^{3/4}$ [Fig. 2(d)].

Experimentally, we study autoresonant dynamics of optical waves in the framework of the photorefractive screening nonlinearity [11], where we employ the induction technique to induce the directional coupler [12] in a 1.2 cm long SBN:75 crystal. Here, the nonlinear index change, $\Delta n_0 = 1/2 n_0^3 r_{33} E \approx 0.0008$, arises from the electro-optic effect, where $E = 1000\ \mathrm{V\,cm^{-1}}$ is the applied field, $n_0 = 2.35$ is the linear refractive index in the medium, and $r_{33} \approx 1200\ \mathrm{pm\,V^{-1}}$ is the relevant electro-optic coefficient. The directional coupler profile is induced by the intensity-superposition of two mutually-uncorrelated ordinarily-polarized Gaussian beams of 10 μm FWHM each. The two beams are separated by $\sim$16 μm, which yields $\kappa \approx 2\ \mathrm{cm^{-1}}$, and we approximate the nonlinearity strength to be $\chi \approx 12\ \mathrm{cm^{-1}}$ [for which $\kappa\chi^{1/2}$ yields 0.007 in normalized units]. One of the beams passes through a gradient-intensity mask to create the chirped waveguide. We place the mask such that the intensity of the beam passing through it increases from 50% to 100% over 1.2 cm, which gives $\Lambda_0 \approx 30\ \mathrm{cm^{-2}}$. The two beams illuminate the crystal in a direction perpendicular to z. Figure 3(a) shows schematics of the experimental setup. The side planes show the intensity profiles of the beams inducing the chirped coupler, and the front (rear) plane shows the intensity profile at the input (output) planes. Figures 3(b) and 3(c) show a 3D intensity image, and the intensity profile inducing the coupler at several propagation planes, respectively. With this index structure, we study the autoresonance dynamics by launching a 1D 10 μm FWHM extraordinarily-polarized Gaussian beam into the right waveguide [black solid line in Fig. 3(c)]. In an unchirped coupler (in the absence of the gradient-intensity mask), we observe complete power transfer and even partial power flow back to the initial waveguide (not shown due to space limitations). Figure 4(a) shows the output intensity profile from the chirped coupler at various values of initial intensity, I (I is in units of the background illumination [11]). At low intensities, as the system crosses the linear resonance, some power tunnels to the left wave-

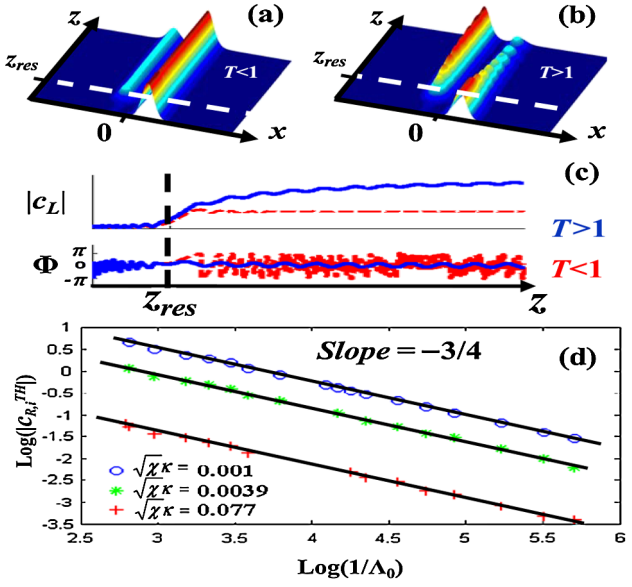

FIG. 2 (color online). Evolution of $|\psi|^2$ (a) below ($T < 1$) and (b) above ($T > 1$) the threshold. White dashed line marks the linear resonance. (c) Dynamics of $|c_L|$ and Φ below (red dashed line) and above (blue solid line) the autoresonance threshold. (d) Threshold amplitude for autoresonant evolution, $|c_{R,i}{}^{TH}|$, versus $1/\Lambda_0$ for different values of $\chi^{1/2}\kappa$. As predicted, $|c_{R,i}{}^{TH}|$ scales as $(\Lambda_0)^{3/4}$.

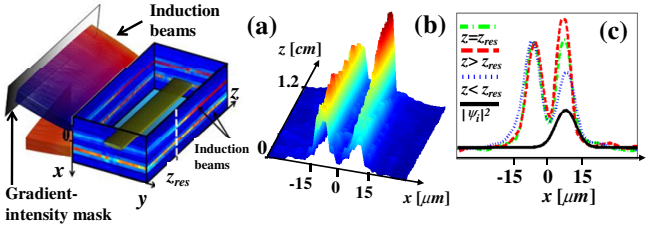

FIG. 3 (color online). *Experimental scheme.* (a) Experimental setup. Side planes depict the intensity profiles of the induction beams, and front (rear) plane shows the intensity profile at the input (output) planes. (b) 3D image of the intensity inducing the chirped coupler. (c) The intensity profile inducing the index change at several propagation planes. Black solid line marks the 1D 10 μm FWHM beam launched into the right waveguide.

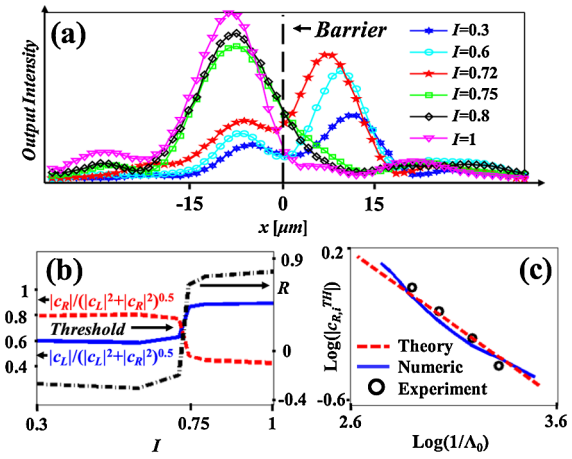

FIG. 4 (color online). *Experiments.* (a) Output intensity profile at several values of initial intensity, I. At low intensities some power tunnels to the left waveguide, but most of the power remains in the right one $I < 0.73$. Above a sharp threshold ($I \sim 0.73$), power transfer becomes efficient and all the power initially launched into the right waveguide emerges from the left one $I > 0.73$. (b) Measured $|c_R|$ (red dashed line), $|c_L|$ (blue solid line) normalized by $|c_R|^2 + |c_L|^2$ and R (black dotted-dashed line), at the crystal output, for various initial intensities. (c) Threshold amplitude for autoresonant phase locking, $|c_{R,i}{}^{TH}|$ as a function of $1/\Lambda_0$. Black circles are the experimental data, the red dashed line is the theoretical threshold for $\kappa\chi^{1/2} \approx 0.007$, and the blue solid line is a numeric simulation of Eq. (1).

guide, but most of the power remains in the right one [$I <$ 0.73 in Fig. 4(a)]. Above the autoresonance threshold ($I \sim$ 0.73), the power transfer process becomes efficient, and all of the power initially launched into the right waveguide emerges from the left one [$I > 0.73$ in Fig. 4(a)].

It is now instructive to show that, as the system crosses the threshold, R increases sharply, and then maintains its high value for increasing intensities. To illustrate this, we calculate $|c_{R,L}|$ (normalized by $|c_R|^2 + |c_L|^2$) and R at the output, for several initial intensities [Fig. 4(b)]. As the system crosses the threshold, $|c_R|$ ($|c_L|$) abruptly decreases (increases) and maintains its value for increasing intensities [red dashed and blue solid lines, respectively]. This result is expressed in a sharp jump in R [black dotted-dashed line], which rises to almost unity. We examine $|c_{R,i}{}^{TH}|$, the threshold amplitude for autoresonant phase locking, by varying Λ_0, and measuring the input amplitude necessary for crossing the threshold. The results are presented in Fig. 4(c) [black circles are the experimental data, the red dashed line is the theoretical threshold, and the blue solid line is the numerical simulation of Eq. (1)]. As expected, for a decreasing chirp rate [increasing $1/\Lambda_0$], the input amplitude required for autoresonant phase locking decreases. The small deviations from the theoretical curve, in both the experiment and the simulation, arise mainly from effects neglected in the coupled-mode theory, e.g., coupling to radiation or to higher modes of the waveguides, waveguide imperfections, etc.

In conclusion, we presented the first study of autoresonance in optics. Autoresonant phase locking of optical waves suggests many new directions. For example, it can play an important role in optically-controlled unidirectional devices for optical switching, in phase locking and amplification in various frequency regimes [visible, soft x-ray, Terahertz], in self-synchronization between optical oscillators [lasers], in efficiency enhancement in various light-matter interactions, and more. Furthermore, it would be interesting to study how autoresonance affects dynamic processes that were studied recently, such as coherent destruction of tunneling in a modulated directional coupler [13], dynamic localization in periodic curved waveguide arrays [14], stimulated Raman adiabatic passage [15], adiabatic sum frequency conversion [16], grating-assisted phase matching in extreme nonlinear optics [17] and more. In addition, it would be exciting if autoresonance could enable efficient frequency conversion in an evolving environment where the structure varies during propagation in a nonprescribed fashion. It might be possible to use autoresonance to force self-phase locking for harmonic generation in a medium where dispersion is random or unknown, as long as it varies adiabatically. We emphasize that autoresonant phase locking is insensitive to the actual form of the chirp as long as it is sufficiently slow.

This work was supported by the Israel Science Foundation (ISF), by the US-Israel Binational Science Foundation, and by an Advanced Grant from the European Research Council.

[1] M. Deutsch *et al.*, Phys. Fluids B **3**, 1773 (1991).
[2] M. S. Livingston, *High-Energy Particle Accelerators* (Interscience, New York, 1954).
[3] L. Friedland and A. G. Shagalov, Phys. Rev. Lett. **85**, 2941 (2000).
[4] L. Friedland and A. G. Shagalov, Phys. Rev. Lett. **81**, 4357 (1998).
[5] B. Meerson and L. Friedland, Phys. Rev. A **41**, 5233 (1990).
[6] A. I. Nicolin *et al.*, Phys. Rev. E **75**, 036208 (2007).
[7] O. Naaman *et al.*, Phys. Rev. Lett. **101**, 117005 (2008).
[8] L. Friedland, Phys. Rev. Lett. **69**, 1749 (1992).
[9] A. Yariv, *Quantum Electronics* (Wiley, New York, 1989), 3rd ed..
[10] L. Friedland, Phys. Rev. E **58**, 3865 (1998); J. Fajans and L. Friedland, Am. J. Phys. **69**, 1096 (2001).
[11] M. Segev *et al.*, Phys. Rev. Lett. **73**, 3211 (1994); J. Opt. Soc. Am. B **13**, 706 (1996).
[12] N. K. Efremidis *et al.*, Phys. Rev. E **66**, 046602 (2002); J. W. Fleischer *et al.*, Nature (London) **422**, 147 (2003).
[13] G. Della Valle *et al.*, Phys. Rev. Lett. **98**, 263601 (2007).
[14] S. Longhi *et al.*, Phys. Rev. Lett. **96**, 243901 (2006).
[15] S. Longhi *et al.*, Phys. Rev. B **76**, 201101 (2007); Y. Lahini *et al.*, Phys. Rev. Lett. **101**, 193901 (2008).
[16] H. Suchowski *et al.*, Phys. Rev. A **78**, 063821 (2008).
[17] O. Cohen *et al.*, Phys. Rev. Lett. **99**, 053902 (2007).